STRESS INDUCED BIREFRINGENCE OF POLARIZATION MAINTAINING FIBERS

Moustafa H. Aly , Ashraf S. Farahat, M.S. Helmi and M. Farhoud

* Faculty of Engineering, University of Alexandria, Alexandria, Egypt
Member of the Optical Society of America (OSA).

Faculty of Science, University of Alexandria, Alexandria, Egypt

Abstract

Both side tunnel and side pit fibers are presented as polarization maintaining fibers fabricated with stress applying zones (SAZs), where birefringence can be achieved because of the elasto-optical effect.

The method of the displacement potential has been applied in both the side tunnel and the side pit fibers to get stresses and consequently birefringence for both fibers.

It was found that the birefringence has its maximum value at the core boundary and decreases towards the SAZ and the core centers.

1. Introduction

Single-mode optical fibers that can maintain the state of polarization over long length are desirable for use in coherent optical communications and fiber optic sensing systems [1]. Single mode fibers, capable of transmitting power in only one polarization state, also have an advantage in interconnecting single mode fibers and polarization-sensitive devices such as integrated optical multiplexers and switches. It is shown by several authors [2] that, in order to make the state of polarization stable, it is an effective measure to freeze anisotropic thermal stress in optical fibers which is greater than the stress caused by external forces. In non-circular core single mode fibers, the difference of propagation constants along two orthogonal directions is introduced by geometrical anisotropy in the fiber cross section and material birefringence due to the residual thermal stress [1].

There are two kinds of polarization maintaining (PM) fibers. The first is the asymmetric geometric high birefringent fiber, and the second is the stress-induced high birefringent fiber. This kind of fiber is fabricated with stress applying zones (SAZ's) so that a particular stress status can be maintained in the fiber. Hence, its birefringence can be achieved because of the elasto-optical effect. The panda, the side tunnel, the side pit and the bow-tie fibers all belong to this category [3].

In this work, both side tunnel and side pit fibers are presented through the application of the thermo-elastic potential method and their material birefringence is studied.

2. Model and Analysis

2.1 Stress Calculation

The function of the stress is to change the intrinsic glass refractive index. Stresses caused by the differential thermal expansion coefficients, α, in different regions of the fiber cross section are calculated using the thermo-elastic potential method [4].

2.2 Thermo-elastic potential method

The stress calculation in an infinite cylinder is a two-dimensional plain strain problem in which the axial strain is assumed to be zero. Thus, the total (thermo-elastic) strain, e, is the algebraic sum of its x and y components. This strain and the displacements, u and v, are related to the product αT across the fiber cross section by [5]:

$$\frac{\partial e}{\partial x} + (1-2\upsilon)\nabla^2 u = 2(1+\upsilon)\frac{\partial \alpha T}{\partial x} \quad , \qquad (1)$$

$$\frac{\partial e}{\partial y} + (1-2\upsilon)\nabla^2 v = 2(1+\upsilon)\frac{\partial \alpha T}{\partial y} \quad , \qquad (2)$$

where T is the absolute temperature of the constituent material in the fiber, and υ is Poisson's ratio. Using the *Goodier* thermo-elastic displacement potential $\Phi(x,y)$ Eqs.(1) and (2) can be combined to Poisson's equation:

$$\nabla^2 \Phi(x,y) = \frac{1+\upsilon}{1-\upsilon}\alpha T \quad , \qquad (3)$$

The solution of Eq. (3) is the particular solution of Eqs.(1) and (2). To obtain the complementary function, the *Airy's* stress function F(x,y) is used [5]. After algebraic manipulation including changing to polar coordinates, one can get the radial stress component, σ_r, the circumferential stress component, σ_θ, and the shear stress component, $\sigma_{r\theta}$ in terms of the total potential $\chi(r,\theta)$ as:

$$\sigma_r = \frac{-E}{1+\upsilon}\frac{T}{r}\left[\frac{\partial \chi(r,\theta)}{\partial r} + \frac{\partial^2 \chi(r,\theta)}{r \partial \theta^2}\right] \quad , \qquad (4)$$

$$\sigma_\theta = \frac{-E}{1+\upsilon}\frac{\partial^2 \chi(r,\theta)}{\partial r^2} \quad , \qquad (5)$$

$$\sigma_{r\theta} = \frac{E}{1+\upsilon}\frac{\partial}{\partial r}\left[\frac{1}{r}\frac{\partial \chi}{\partial \theta}\right] \quad , \tag{6}$$

subject to the boundary conditions:

$$\sigma_r = \sigma_{r\theta} = 0 \qquad \text{at } r = b \tag{7}$$

2.3 Birefringence Calculation

Having found the stresses, the corresponding material birefringence, B_s, can be obtained as [6]:

$$B_s = (c_1 - c_2)\left[(\sigma_r - \sigma_\theta)\cos 2\theta - 2\sigma_{r\theta}\sin 2\theta\right] \tag{8}$$

where c_1, c_2 are the elasto-optical coefficients of the fiber material.
The effective birefringence, B_e, can be evaluated through its definition [7]:

$$B_e = (c_1 - c_2)(\sigma_x - \sigma_y)_e \ , \tag{9}$$

Where

$$(\sigma_x - \sigma_y)_e = \frac{\int_0^{2\pi}\int_0^{\infty}\left[\sigma_x(r,\theta) - \sigma_y(r,\theta)\right]E^2 r\,dr\,d\theta}{\int_0^{2\pi}\int_0^{\infty} E^2 r\,dr\,d\theta} \tag{10}$$

with E the electric field of the HE_{11} mode.

The structure of the side tunnel fiber is shown in Fig.1. The thermal expansion coefficients of the core, the SAZ's and the remainder of the cladding are α_1, α_2, α_2, respectively.

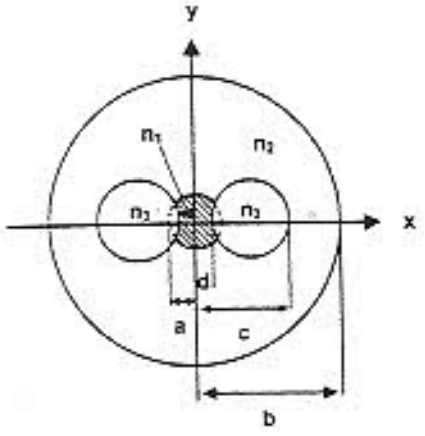

Fig.1 side tunnel fiber

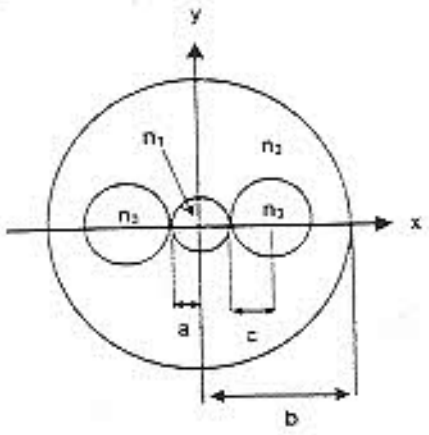

Fig.2 side pit fiber

To obtain the thermo-elastic displacement potential $\Phi(r,\theta)$, the term α is replaced by $(\alpha_1-\alpha_2)$ in the core region and by $(\alpha_2-\alpha_3)$ in the SAZ. Introducing the temperature effect, stresses at any point through the core due to the contribution of the displacement potential are obtained as:

$$\sigma_r{}^{\Phi} = \frac{-ET}{2(1+\upsilon)}\left\{\beta_1 + \beta_3\left(\frac{c-b}{2}\right)^2\left[\frac{x_1}{x_3{}^2} + \frac{x_2}{x_4{}^2}\right]\right\} \ , \tag{11}$$

$$\sigma_\theta{}^{\Phi} = \frac{-ET}{2(1+\upsilon)}\left\{\beta_1 + \beta_3\left(\frac{c-b}{2}\right)^2\left[\frac{2x_3 - x_5{}^2}{x_3{}^2} + \frac{2x_4 - x_6{}^2}{x_4{}^2}\right]\right\} \tag{12}$$

$$\sigma_{r\theta}{}^{\Phi} = \frac{-ET}{2(1+\upsilon)}\beta_3\left(\frac{c+2b}{2}\right)\left(\frac{c-2b}{2}\right)^2 \sin\theta\left[\frac{x_5}{2x_3{}^2} - \frac{x_6}{2x_4{}^2}\right] \tag{13}$$

where E is Young's modulus, and x_i's are functions of the fiber dimensions b, c and d and the propagation constants β_1 in the core and β_3 in the SAZ.
In a similar manner, the SAZ's stresses due to the displacement potential are obtained as:

$$\sigma_r{}^{\Phi} = \frac{-ET}{2(1+\upsilon)}\left[\frac{\beta_1 a^2}{r^2} + \beta_3\left[1 + \left(\frac{c-b}{2}\right)^2\frac{x}{y^2}\right]\right] \ , \tag{14}$$

$$\sigma_\theta{}^{\Phi} = \frac{ET}{2(1+\upsilon)}\left[\frac{\beta_1 a^2}{r^2} + \beta_3\left[-1 + \left(\frac{c-b}{2}\right)^2\frac{x}{y^2}\right]\right] . \tag{15}$$

$$\sigma_{r\theta}^{\Phi} = \frac{ET}{2(1+\upsilon)}\beta_3\left(\frac{c-b}{2}\right)^2\left(\frac{c+2b}{2}\right)\frac{z}{y^2}\sin\theta \quad (16)$$

where x,y,z are x_2, x_3, x_4 for the right lobe ,x_1, x_3, x_5 for the left lobe.

In the cladding region the stresses are derived as:

$$\sigma_r^{\Phi} = \frac{ET}{2(1+\upsilon)}\left\{\frac{\beta_1 a^2}{r^2} + \beta_3\left(\frac{c+b}{2}\right)^2\left[\frac{x_1}{x_3^2} - \frac{x_2}{x_4^2}\right]\right\} \quad (17)$$

$$\sigma_\theta^{\Phi} = -\sigma_r^{\Phi} \quad (18)$$

$$\sigma_{r\theta}^{\Phi} = \frac{-ET}{2(1+\upsilon)}\beta_3\left(\frac{c-b}{2}\right)^2\left(\frac{c+2b}{2}\right)\sin\theta\left[\frac{x_5}{2x_3^2} - \frac{x_6}{x_4^2}\right] \quad (19)$$

The second fiber in this study is the side pit fiber, Fig.2. The same procedure is repeated for this fiber but the term (c + b)/2 is replaced by (c + a) and the term (c – b)/2 by (c). Here a, b and c are, respectively, the radii of core, clad and SAZ.

The described method of the displacement potential has been applied in both the side tunnel and the side pit fibers to get stresses and birefringence for both fibers. The fiber parameters used are listed in table I.

Table I Parameters for side tunnel and side pit fibers

	Side tunnel fiber	side pit fiber
2a (μm)	5 – 10	15.6
2b (μm)	125	125
B/c a/b	0.15 2.0 – 4.0	-
α_1 ($^\circ C^{-1}$) α_2 ($^\circ C^{-1}$) α_3 ($^\circ C^{-1}$)	7.6×10^{-6} 5.4×10^{-7} 3.66×10^{-5}	9.4×10^{-7} 5.4×10^{-7} 10.5×10^{-7}
T (°C)	-1000	-650
E (kg/mm^2)	7830	7830
v	0.186	0.186
$c_1 - c_2$ (mm^2/kg)	3.36×10^{-5}	3.36×10^{-5}
2c (μm)	-	30
d_x(μm)	-	2.28×10^{-6}

3. Results and Discussion

It can be observed from Figs. 3 and 4 that the residual stresses inside the core are nearly constant and independent of the radial distance. One can also observe that the difference between the radial and tangential stresses is constant and independent of the cylindrical coordinates r and θ. For this reason, the material birefringence is slightly different from point to point in the core as shown in Fig.5. The results of Fig.5 show the same behavior as obtained for the same fiber by the method of finite element [1].

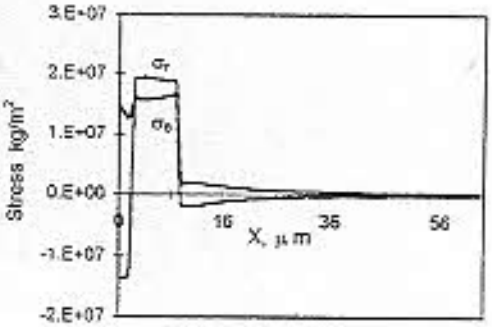

Fig 3 Radial and tangential stresses along X-axis in a side tunnel fiber.

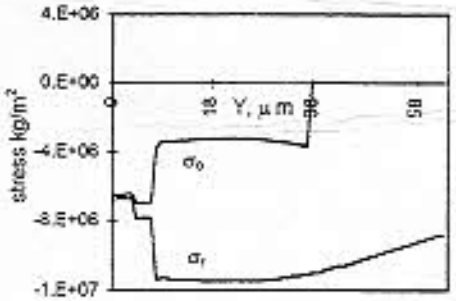

Fig 4 Radial and tangential stresses along x-axis in the side tunnel fiber.

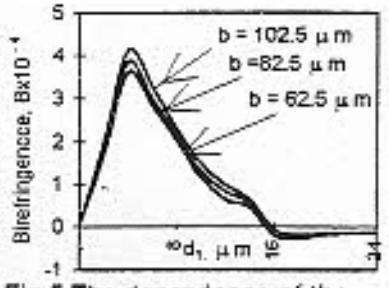

Fig 5 The dependance of the material birefringence, B on d_1, at different cladding radius, b for the side tunnel fiber.

The presence of the SAZ's affects the stresses along the x-axis in the cladding region, where the difference between radial and tangential stresses decreases with radial distance. However, along the y-axis, this difference is nearly the same at all points.

Figure 5 shows the dependence of the material birefringence on d_2. Two representations of the birefringence are observed; B_{av} and B_e. The first is the average birefringence taken through the core area after dividing it into small cells. The second is the effective birefringence, B_e, which is considered to be the most accurate because it does not ignore the influence of the wavelength dependence of the optical field. It is noted that the birefringence has its maximum value at the core boundary and decreases towards the SAZ and the core centers. This can be explained by the influence of the SAZ's.

In Figure 6, one can observe a direct proportionality between the birefringence and both the SAZ area and the cladding radius till the core boundary and then the relation is reversed to be indirect proportionality.

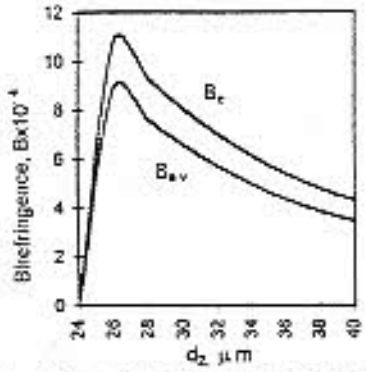

Fig 6 The diffeerent representations of the material birefringence B, on d_2 in the side tunnel fiber.

Figures 7 and 8, for the side pit fiber, show nearly the same behavior like the side tunnel fiber. For the x- axis dependence, near the core boundary the difference between radial and tangential stis more significant. In the first region of the clad, both stresses have nearly constant values. For the y-axis dependence radial and tangential stresses are nearly constant in the core region then become closer to each other as shown in Fig. 8. Figure 9, for the side pit fiber, shows the same behavior as the side tunnel fiber. Results in Figs. 9 and 10, for the side pit fiber, are similar to that obtained for side tunnel fiber.

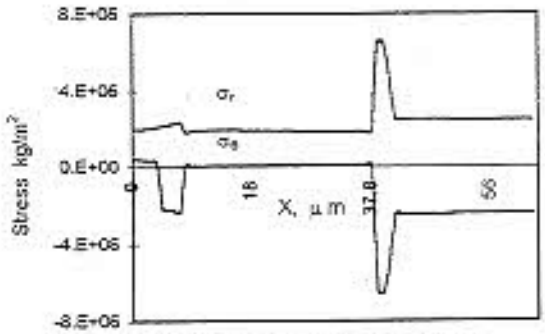

Fig 7 Radial and tangential stresses along x-aixs in a side pit fiber.

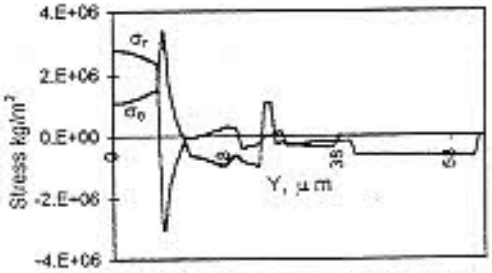

Fig 8 Radial and tangential stresses along y-axis in the side pit fiber.

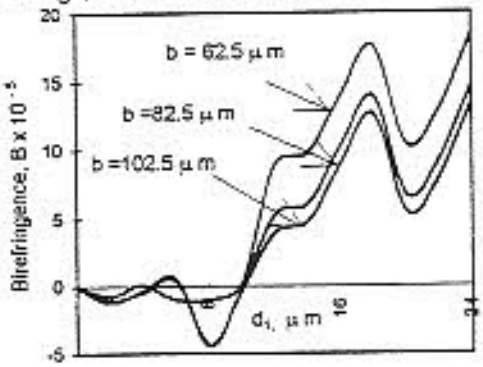

Fig 9 The dependance of the material birefringence b, on d_1, for the side pit fiber

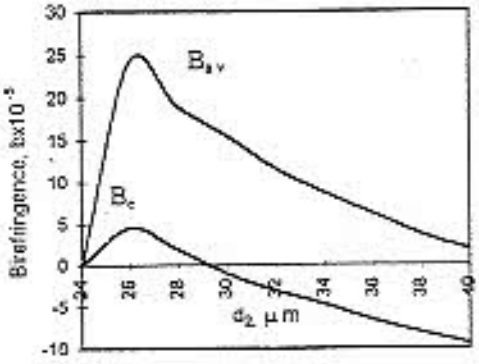

Fig 10 The different representations of the material birefringence B. on $d_2$in the side pit fiber

4. Conclusion

The method of the displacement potential has been applied in both the side tunnel and the side pit fibers to get stresses and birefringence for both fibers.

It was found that the residual stresses inside the core are nearly constant and independent of the radial distance. It also was found that the difference between the radial and tangential stresses is constant and independent of the cylindrical coordinates.

It was also found that the birefringence has its maximum value at the core boundary and decreases towards the SAZ and the core centers.

References

1] Katsunari Okamoto, Toshihito Hosaka, and Takao Edahiro, " Stress Analysis of Optical Fibers by a Finite Element Method". IEEE J. Quantum Electron. , Vol. QE-17, No 10, 1981.

2] P. Daly, "Finite element approach to propagation in elliptical and parabolic waveguides," Int J. Num. Meth. Eng., vol 20, pp. 681-688, 1984.

3] T. Okoshi & K. Kikuchi, "Heterodyne-Type Optical Fiber communications.", J. Opt commun., Vol. 2, No. 3, pp. 82-88, 1981.

4] Danny Wong & Pak Lim Chu, "Stress Calculations Based on Point Matching Method for Mechanically Inhomogeneous Optical Fibers", IEEE J. lightwave technol., vol. LT-9(1), pp. 37-47, 1991.

5] S. P. Timoshenko & J. N. Goodier, "Theory of Elasticity", 3rd ed., New York: Mcgrow-Hill, 1970.

6] Kazuya Hayata, Masanori Koshiba, " Stress-induced Birefringence of Side-Tunnel Type Polarization-Maintaining Fibers", IEEE J. lightwave technol., vol. LT-4, 1986.

7] Juichi Noda, Katsunari Okamoto & Yutaka Sasaki, "Polarization-Mainyaing Fiberrs and Their Applications", IEEE J. lightwave technol., vol. LT-4(8), pp.1071-1089, 1986.